An insight study into the parameters altering the emission of a covalent triazine framework

Panagiota Bika[a], Tatiana Giannakopoulou [a], Vitaly Osokin[b], Mo Li[c] , Nadia Todorova[a], Andreas Kaidatzis[a] , Robert A. Taylor[b], Christos Trapalis[a] and Panagiotis Dallas*[a]

Covalent triazine frameworks (CTFs) synthesized through nucleophilic substitution of 4,4' bipyridine on the carbon atoms of cyanuric chloride were studied as fluorescent sensors. The band gap of the materials was calculated to be 2.95 eV from diffuse reflectance measurements, while from the adsorption in aqueous dispersions, we obtained the value of 3.7 eV. A partial exfoliation of the layered CTFs in water or tetrahydrofuran led to different morphologies, increased emission lifetime and fluorescence quantum yield. The pattern of their light emission properties in combination with their redox states was defined with the addition of a series of acidic and basic analytes. Another unique aspect of these semiconducting materials is the induced aggregation and the subsequent enhancement of emission under ultraviolet illumination.

Introduction

Covalent organic frameworks (denoted as COFs) are porous and crystalline 3D architectures with numerous applications, such as electrochromic device components[1–3], sensors[4–8], photocatalysts and electrocatalysts[9–12], energy storage[13,14], separation membranes[15], supercapacitors[16] and templates for heavy metal extraction[17]. The broad scientific interest on these sp^2 conjugated polymers had intrigued many advances with new types of synthesis arising as the low temperature polycondensation approach[18] and new types of hollow spheres[19] morphologies that deviate from the planar sheets or tube structures. Their potential enables a wide range of functionalities. For example, regarding their sensing ability, viologen-based COFs offer a visual detection of substances, guest molecules[8,20], O_2[21], humidity[6,22], temperature[5] and even UV light. A further modification to hybrids and nanocomposites with inorganic materials, nanoparticles, and graphene sheets is highly anticipated for the enhancement of the physical properties of the COFs.

When the frameworks are consisted of a central triazine core, they fall under the designation of covalent triazine frameworks (CTFs)[23]. Numerous methods exist for their synthesis that provide pre-designable and precise final structures. The characteristics that establish them as adaptable platforms for multi-functional materials, are first and foremost their chemical versatility, due to the covalent nature of their bonds, their high π-π conjugation, as well as high porosity, surface area, and tuneable properties[24].

Methyl viologen and its derivatives are versatile building blocks for the synthesis of COFs with very interesting paramagnetic and optical properties[25]. The electronic and adsorption properties of viologen derivatives are widely known, but their emissive response in combination with the electron deficient triazine centre[26] has not been thoroughly studied. Recently, covalent networks with light emitting properties have been used as sensors for the detection of metals, based on a shift of the emission maxima and intensity[27,28]. The sensitivity of these materials to light alternations is the consequence of physicochemical and structurally endured transformations, that is a prominent characteristic of photochemical molecules similar to azobenzenes[29].

Herein, we report the tuning of the light emitting properties of bipyridine-triazine networks by means of concentration, irradiation, and alkaline or acidic media in aqueous dispersions. The materials were synthesized in a THF solution through a nucleophilic substitution of the triazine core with 4,4' bipyridine. A subsequent soft chemical exfoliation happened through ion exchange with SDS and moreover a mechanical exfoliation was succeeded through dispersion and sonication in liquid environments. The resultant exfoliated CTFs entailed a variation of morphologies with increased fluorescence and emissive lifetime. Structural alterations provoked locally by the different redox states under UV irradiation spread through the continuous crystallographic network giving rise to new adaptable and multifunctional semiconducting materials.

Materials and methods

Synthesis of the covalent triazine framework (CTF)

[a] *Institute of Nanoscience and Nanotechnology, National Centre for Scientific Research "Demokritos", 15341 Athens, Greece.*
[b] *Department of Physics, Clarendon Laboratory, University of Oxford, Parks Road OX1 3PU, United Kingdom.*
[c] School of Electronic Science and Engineering, University of Electronic Science and Technology of China, Chengdu 640054, China
† Corresponding author: p.dallas@inn.demokritos.gr.
Electronic Supplementary Information (ESI) available: [details of any supplementary information available should be included here]. See DOI: 10.1039/x0xx00000x

The chemical reagents of cyanuric chloride (99.9%), Tetrahydrofuran (>99.9%) were purchased from Sigma Aldrich and 4,4' bipyridine from Alfa Aesar (98%). The bulk CTF (b-CTF) was synthesized step by step according to Bourlinos et al.[30], and the nucleophilic substitution happened under reflux at 100 °C in THF instead of toluene. The condensation polymerization proceeded to the formation of the framework. The yield of the reaction was 100% and the greenish powder was collected and kept in vials in the dark. The molecular weight of the CTFs repeated building blocks was calculated at 358 g/mol. All calculations are considering the molecular weight of the repeated building block and not of the polymeric framework. The characterization of the b-CTFs was performed for their solid state and their dispersions in different solvents (b-CTF/H_2O, b-CTF/THF, b-CTF/MeCN, b-CTF/C_2H_6O, b-CTF/C_3H_8O).

Exfoliation of CTFs

The b-CTF powder was dispersed in de-ionized H_2O or THF to perform the mechanical exfoliation. A 12-hour bath sonication process was enough to exfoliate 20 mg of each material in 100 ml of solvent. The transparent supernatant solutions were left to evaporate at room temperature (RT) and the precipitated quantities were disposed. The dry exfoliated samples (dark-green exfoliated in H_2O and dark-brown exfoliated in THF) were collected and kept in Eppendorf tubes in the dark. Their solutions were denominated according to the solvent used for their exfoliation, that is, exf-CTF(H_2O) and exf-CTF(THF), throughout the article. Regarding the chemical exfoliation with the sodium dodecyl sulfate (SDS), the procedure is described at the previously published paper by Bourlinos et al. [30].

Titration of CTF dispersions

Titrations with salts, oxides, bases, oxidative and reducing agents took place for two different concentrations of b-CTF/H_2O (5.6×10^{-4} M and 2.35×10^{-5} M of CTF) dispersions. The addition of the reagents was made either with molecular equivalence or in excess to the CTF for an effective comparison.

Characterization techniques

Fourier Transform Infrared (FTIR) spectra for the solid samples were measured on a Thermo Nicolet iS50 instrument in attenuated total reflection mode from 400 cm^{-1} to 4000 cm^{-1}. X-ray diffraction (XRD) patterns were completed in the 2θ range of 2-60° with a Siemens D500 X-ray diffractometer, using Cu-K_a radiation (λ=1.5418 Å) for powders and films deposited on glass substrates. Scanning electron microscopy (SEM) and FEI inspect microscope equipped with tungsten filament operating at 25 kV were used to investigate the morphology of the semiconducting powders, which were beforehand sputter-coated with Au. A NT-MDT NTEGRA Atomic force microscope (AFM) was employed for topological imaging, in non-contact mode with commercial SPM probes (Nanosensors PPP-FMR.). Si <100> wafers of 1 cm x 1 cm were used for the single-layer deposition of dispersions by spin coating prior to the measurements. All the obtained AFM images were processed using the WSxM software. Liquid N_2 adsorption/desorption isotherms were obtained with a Quantachome Autosorb-iQ instrument. The specific surface area and pore size distribution were determined applying BET and BJH methods on adsorption and the desorption branch, respectively. The electrochemical behavior of the prepared materials was evaluated using a Metrohm Autolab PGSTAT302 potentiometer in conjunction with a beaker type three-electrode cell via cyclic voltammetry (CV) and electrochemical impedance spectroscopy (EIS). To perform the measurements, a counter (Pt sheet), a reference (Ag/AgCl, 3M KCl) and a working (Glassy carbon covered with the investigated material) electrodes were embedded into a 0.2 M NaCl solution (pH ~ 5.8). The electrode material was prepared in a typical way[31], when 10 mg of investigated material was dispersed in 0.5 ml of distilled water, and after that 25 μl of the prepared dispersion was dropped on the GC electrode and left to evaporate. The CV measurements were performed in a potential range from -1.0 V to 1.0 V or 2.0 V where appropriate with a scan rate of 50 mV/s. Zeta potential measurements were performed on a Malvern Instruments Zetasizer Nano™ Series analyzer and each powder was dispersed in water. UV-Visible diffuse reflectance and absorbance spectra were carried out on a Shimadzu UV-2100 spectrophotometer with an integrating sphere and quartz cuvettes, respectively. Excitation dependent photoluminescence (PL) spectra were obtained on a JASCO FP-8300 spectrofluorometer. The sensitivity was set at the low level for measurements used for the quantum yield calculations. Time resolved photoluminescence was measured with a Janis microscope cryostat (ST-500) from 5 to 300 K on silicon wafers for both the pristine materials and the exfoliated samples, before and after 30 min of UV irradiation. The wavelength of excitation was between 370 nm and 405 nm using a frequency tripled 100 fs Ti:Sapphire laser operating at a repetition frequency of 76 MHz. The emission was detected using a PicoQuant TimeHarp time-correlated single photon counting system and a photomultiplier tube with an instrument response function of 150 ps. Thin films were spin coated onto Si wafer substrates at 1000 rpm for 30 seconds on a WS-650 series spin processor by Laurell Technologies Corporation®. After 5 depositions of the dispersions with the same spin coating parameters, the 5-layered films were obtained. The presented molecular structure of the CTFs was designed with the Chemdraw software.

Results and Discussion.

Structural and chemical characterization. Evolution of different morphologies and arrangement of the layers.

The nucleophilic substitution of the chlorine atoms in cyanuric chloride by 4,4' bipyridine bridges formed two dimensional networks through quaternarization of the nitrogen atoms[30]. The network is composed of central 1, 3, 5-triazine units covalently linked with 4,4' bipyridinium rings, extending in a large 3D scale throughout the material. The presence of the Cl^- as counter ions, contributes to the structure by the formation of outer sphere charge-transfer complexes[32]. 4,4' bipyridine possesses three different redox states: with the formation of free radicals,

certain stereo chemical changes are occurring in the networks, in parallel with the existence of either positive-charged (oxidized) or neutral (reduced) nitrogen atoms in its aromatic rings. Their oxidative state has a torsional aromatic structure which converts to a strong quinoid, planar, state when it is fully reduced due to changes in the length and angle of inter-ring C-C bond (Scheme 1). While the dicationic species are hydrophilic, after the generation of radicals through a reduction process or a photo-induced electron transfer, the respective monocations are proven to be more hydrophobic[33]. Nitrogen is found in a slight pyramidal configuration[34],[35] and its lone pairs do not participate in the π-conjugation. 4,4' bypiridine under different stimulations can serve as the electron donor and its bonding with the electron deficient 1,3,5 triazines permits the preservation of higher molecular planar symmetry. The linking molecule displays smaller displacements from layer to layer[36]. π-π stacking distance is also preserved.

The FTIR spectra of the conjugated polymeric bulk and exfoliated CTF materials are identical and the signal of the C-Cl stretching vibration from the cyanuric chloride at 850 cm^{-1} is absent in all cases (Figure S1). The triazine unit and bipyridine vibration modes of heterocyclic rings appear at 1650-1000 cm^{-1} in each spectrum (Figure S1) and the vibration frequencies of

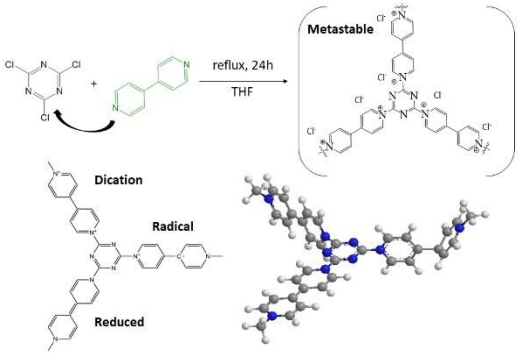

Scheme 1 Nucleophilic substitution of $(NCCl)_3$ with $(C_5H_4N)_2$ leads to a framework bearing chlorine counter ions and free radicals due to extreme electron deficiency of its metastable state. In this scheme, the configurations of one unit of the framework are demonstrated, depending on the redox state of the viologen derivatives. The chlorine ions are omitted for clarity: N: blue, C: grey and H: white atoms.

the exfoliated CTF in H_2O coincide with those in the spectrum of the b- CTF. However, for the exf-CTF(THF), minor differences are observed in the range of 2000-3500 cm^{-1}, signalling a contribution from the residual solvent.

The SEM images and the X-ray diffraction patterns recorded before and after the exfoliation of the materials are presented in Figure 2a, respectively. Structural characterization through X-ray analysis reveals a polycrystalline configuration in the bulk sample with predominant peaks that indicate a π-π stacking-driven assembly at 3.3 Å (2θ=26.8°). This layer-by-layer assembly leads to the formation of extensive blocks of different sizes and its molecular ordering occurs in the direction perpendicular to the 2D planar sheets, with offset alignment in an AB stacked hexagonal crystal system. Its edge-to-edge distance fluctuates with the redox states and small shifts of the reflections can be observed when modifications occur in the environment of the b-CTF. There are numerous intermolecular forces affecting the stabilization of π-π stacking distances between closed-shell molecules, mainly owing to electrostatic and Van-der-Waals interactions as explained by Janiak et al[37].

The partial exfoliation in aqueous dispersions (exf-CTF(H_2O) is apparent from the SEM images (Figure 2a and Figure S2), while the π-π stacking signal in XRD is less intense, with lower crystallinity than b-CTF (Figure 2a). As for the exf-CTF(THF), while AB stacking is lost, the symmetry planes of its lattice are reformed at a final ordered morphology and two new intense reflections appear centred at 19.5° 2θ and 29.5° 2θ. The former peak reflects a periodicity parallel to the densely packed polymer chains with Cl^- ions remaining in between them[30],[38],[39] and the latter one describes the close approach of the carbon atoms to 3.03 Å due to a tilt of several ring planes[37]. These peaks were pre-existing in the b-CTF at a lower intensity, so there is a possibility that this CTF is following Steno's law for the constancy of interfacial angles. In the THF solution, the electrostatic repulsion led to the weakening of π-π interactions between the sheets and thus larger spacing, favouring the intercalation of the solvent. A noncovalent π interaction could be present between the lone pair electrons of electronegative atom of oxygen in THF and the deficient and positive character of C aromatic atoms in s-triazine. SEM images demonstrate this micro-structural conversion from 3D blocks of 2D layers for the bulk and 2D exfoliated flakes of different sizes in polar H_2O, to fine rectangular microcrystals[40] for the exfoliation in THF (Figure 2a). It should be noted that the term 'rearrangement' is more representative than 'exfoliation' when we are referred to the effect of the organic solvent. Both electrostatic repulsion and solvation are important for the aqueous exfoliation and THF rearrangement[41]. The specific surface area (SSA) of the b-CTF determined through BET measurements (Figure S3) was of 4.6 m^2/g. The calculated area is low in comparison to other reported results for CTFs, due to the AB stacking of the sheets and the pore blocking from the counter ions[41]. The exf-CTF (H_2O) demonstrates an order of magnitude higher SSA of 33.4 m^2/g than the b-CTF. The main micro pores with radius of 16 Å correspond possibly to the distance between the two parallel edges of the hexagonal conformation (Figure 2b, Figure S4). The pore size distribution is in agreement with the X-ray diffraction measurement of the b-CTF/H_2O deposited on a glass substrate (Figure 2b), which present a pattern with enlarged intermolecular distances and cavities of 19 Å and 24 Å ((100) plane)[42,43]. A sharp peak appearing at 11.6° 2θ with a d-spacing value of 7.6 Å corresponds to the molecular dimension of 4,4' bipyridine, which is in accordance with the molecular structure a free viologen moiety found at 8.6 Å. The chemical exfoliation by subsequent exchange of the chloride counter ions by sodium dodecyl sulfonate $(C_{12}H_2)_5OSO_3$ results in further expansion of the interlayer space to 3 nm[30].

AFM was employed to further elucidate the morphology and the layer-by-layer structure of the bulk-CTF network. The AFM images are displayed in Figures S5 and S6. A widespread population of flakes is seen with approximately 5 nm height corresponding to 15 layers per flake.

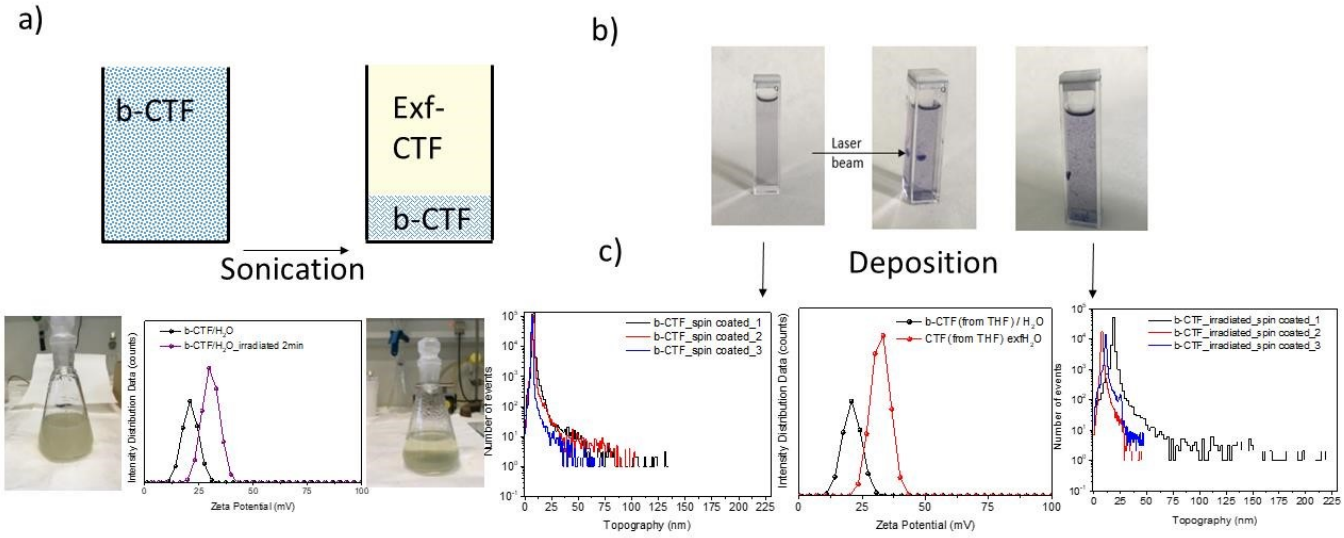

Figure 1 a) Schematic representation of the exfoliation of b-CTF dispersion in H_2O and their respective zeta potential. b) The induced aggregation by UV irradiation in an aqueous dispersion of b-CTF. c) Height histograms obtained from topography images of the single layer depositions on Si wafer from b-CTF dispersion prior and after UV irradiation, alongside with their zeta potential.

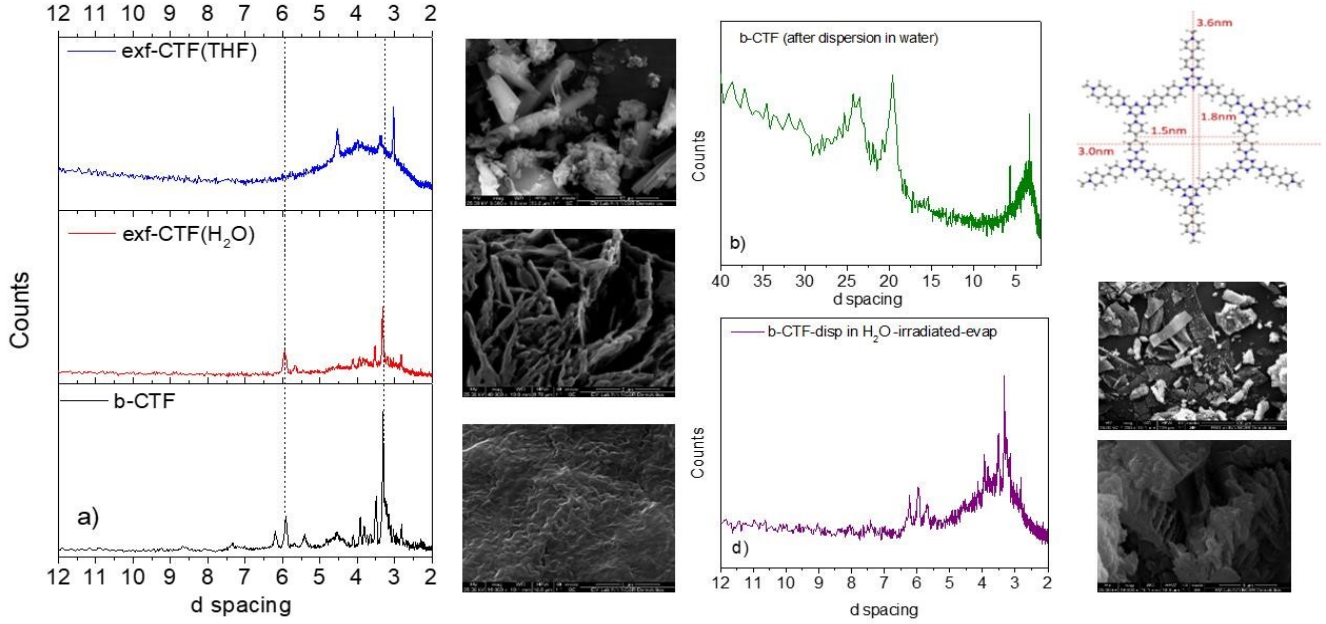

Figure 2 . a) XRD patterns of bulk and exfoliated CTFs powders, b) XRD pattern of the film from b-CTF/H_2O dispersion deposited on glass, c) A representation of a hexagonal unit of the covalent organic/triazine framework composed by 6-triazines and 12-4.4' bipyridines and d) D-spacing of b-CTF irradiated in H_2O.

As demonstrated in Scheme 1, UV irradiation induces changes from a di-cationic to a mono-cationic state. Interestingly, the materials reveal a light induced aggregation in aqueous dispersion under UV irradiation (Figure 1b). Consequently, σ-π attraction may become more pronounced and lead to opaque polymeric assemblies with polycrystalline nature as layers with opposite charges are preferentially approaching each other with an induced AB morphology (Figure 2c and Figure S9). The effect of UV irradiation on the same b-CTF/H_2O was also examined with AFM (Figure 1c, Figures S7 and S8) and revealed an augmentation of the sheets' average height with the most prevailing population found at 24 nm (a sum of 73 layers). These characterization techniques validate at the nanoscale the distortion and the structural changes spreading after irradiation to the whole framework by crystallographic and symmetric operation, thus giving rise to an anisotropic shrink in the three-dimensional crystal packing [44] (Figures S8 and Figure S9).

The redox states of the covalent networks. Electrochemical characterization, UV-Visible absorbance and reflectance.

The b-CTFs are acidic with a pH=3.5, and they are positively charged according to the concentration of the b-CTF in comparison with the concentration of [OH^-] in the solution[45] (Figure S10). Under UV irradiation for 2 minutes, the partial charges existing on the quadrupole alternate. This influences the electrostatic interactions, causes reorganization of the b-CTF structure of the and increases its surface potential to +29.6 mV from the initial +20 mV value of the 1.1×10^{-3} M b-CTF dispersion (Figure 1 and Figure S11), whereas the pH value remains stable.

The cyclic voltammetry measurements of three cycles (Figure 3a) indicate two main oxidation and reduction peaks, while an intermediate one at -0.5 V has been previously assigned to the production of H_2[46] or H_2O_2 peroxide in O_2 saturated solutions[12]. For the redox potentials of the b-CTF on the GC electrode, the reduction of di-cation to radical species is favoured at smaller voltages -0.23 V/-0.11 V and is easier than the reduction of mono-cation species to neutral species[1] at -0.78 V/-0.31 V. A passage from light green to an eye detectable purple-black colour happened in the first semi-cycle from 0 V to -1 V. A further transition from purple-black to red coloration[47] was accomplished during the reduction step of the 2nd cycle, whereas the reversible change occurred during the oxidation steps from -1.0 to +1.0 V. Therefore, the dimerization and comproportionation of viologen moieties of the red coloured b-CTF takes place due to the alternating charges[48]. In order to fully re-oxidize the b-CTF and to reverse it to its initial light green colour, a higher positive voltage of +1.8 V should be applied in the aqueous NaCl solution. When the deposited b-CTF/H_2O was irradiated prior to the CV cycles, small changes of the redox peaks are observed. A higher current at the 1st reduction cycle of the 2nd peak and a higher oxidation voltage for the corresponding peaks exist (Figure 3a) because of the opaque structure developed from the irradiation of the b-CTF, as explained in the previous section. The reversible colour transition made evident the alternation of redox states and charge in the network.

Throughout the years, the three redox states of the methyl viologen derivative had been precisely characterized by UV-vis spectroscopy along with its electron transition behaviour in the solid [3,49] and liquid state[47]. UV irradiation of the solid-state b-CTFs for 30 minutes diminishes the reflectance at λ=490; 530; 610; 660; 850 nm (Figure 3b, Figure S12). The new peaks are assigned to the transition of charge separated states via electron transfer of C_{sp2} to N_{sp2}, which induced intramolecular electronic transfer from and in between chlorine ions and free electron pairs of N atoms, while promoting new interactions in the polymeric network. The green coloured samples are slowly bleached back to their initial lightly coloured state in vials left in the dark, thereby highlighting the auto-reversibility of the effect. The photo-response of the b-CTF powder has a great tolerance at repeated cycles without any variations of the measurements[2].

The absorbance of the b-CTF found in low and high concentrations dispersed in H_2O, as well as for non-irradiated and irradiated dispersions under a UV 370 nm lamp of 20 V/m^2 is presented in Figures 3c and 3d. Generally in the liquid state, MV^{2+} exhibits an absorption at 261 nm its blue coloured radical cation $MV^{+\cdot}$ appear at 397 nm, 608 nm and 732 nm and the yellow coloured MV^0 is located at 401 nm[47]. Its red coloured dimers appear at 368 nm and 537-556 nm[50] and are highly dependent on the concentration[51] of the viologen in aqueous environments. During the dispersion of the b-CTF in H_2O, a reaction with the molecular oxygen is proposed to happen rapidly[52], in addition to an ion exchange with OH^- groups and potentially, a proton transfer. The intensity of the absorbance is increased for the concentrated dispersion within 5 min of UV irradiation (Figure 3d) and the peaks at 390-410 nm, 550 nm and 732 nm are more intensively pronounced than for the diluted b-CTF dispersion (Figure 3c). The solubility of the monocationic structures decreases, and they exhibit a hydrophobic character[53] compared to the b-CTF in the fully reduced state. As distinguished from the spectra of the diluted dispersions (Figure 3d), the peak of 4,4' bipyridine is located at 240 nm and the one of triazine at 270 nm. The new peaks at higher wavelengths, created after the irradiation, are less pronounced here in comparison to the denser dispersion, and their absorption

peaks centred at 390 nm, 410 nm and 550 nm are akin to the irreversible electron transfer from chlorine counter ions to the CTF and to the generation of carbon centred radicals as verified also by EPR[54]. The direct optical band gap of the b-CTF dispersed in H_2O was determined using the absorption function $(a\ h\nu)^2=f(eV)$ and was calculated to be 3.7 eV, confirming its semiconducting nature. The increase of the band gap is due to interaction with H_2O, as the b-CTF isn't found at its aggregated and quenched form.

The solvent environment has a dual role, as both a redox partner and a solvation medium. The polarity of the solvent constitutes the key element for a control over the sensitivity of solvatochromism in viologen systems[7,55]. As it is presented in Figure S13, the higher the polarity of the solvent, the more the absorption spectrum of the b-CTF is red shifted. Colour deviations are also highly associated with the dispersing medium of the CTF, for example, H_2O or in THF. It is likely that ion-pair formation in organic solvents with low dielectric constant, such as THF, precludes the possibility of dimerization[56] in the network. It is already proven that solvents with ionization potential (IP) lower than 10.8 eV tend to be oxidized by electron transfer from the excited viologen units, quenching the absorption and therefore the emission of the CTF[57,58].

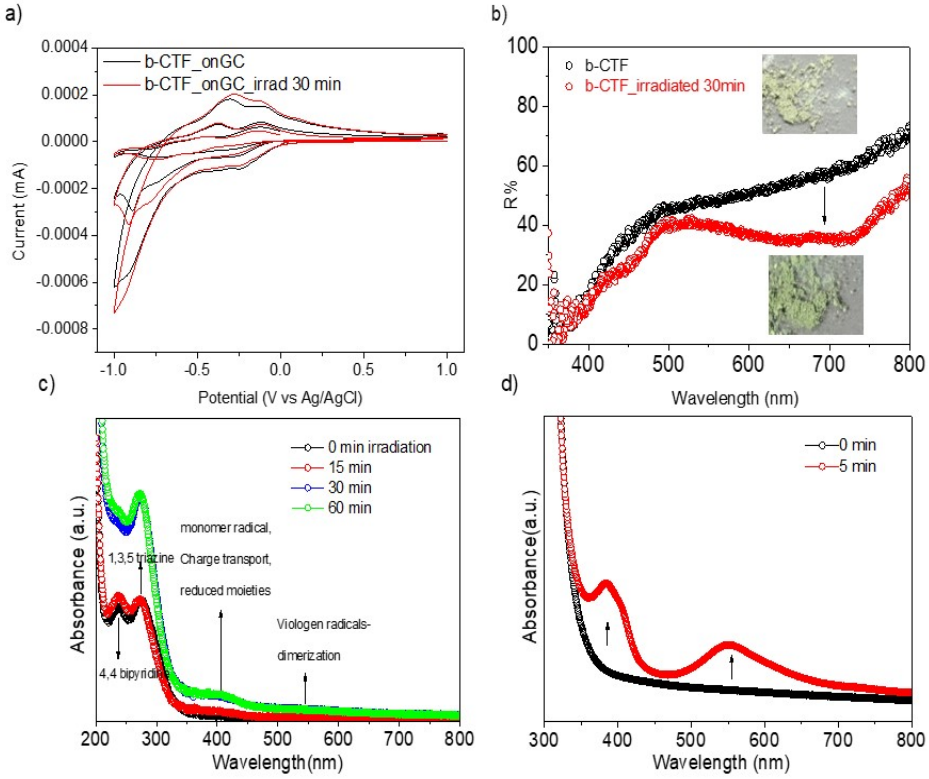

Figure 3. a) Cyclic voltammetry of b-CTF dispersed in H_2O and deposited on GC electrode before and after 30 min of UV irradiation, b) Diffuse reflectance spectra of b-CTF in the solid state before and after UV irradiation, c-d) UV-visible spectra of b-CTF in aqueous dispersions at 9.5×10^{-5} M and 5.6×10^{-4} M, before and after UV irradiation

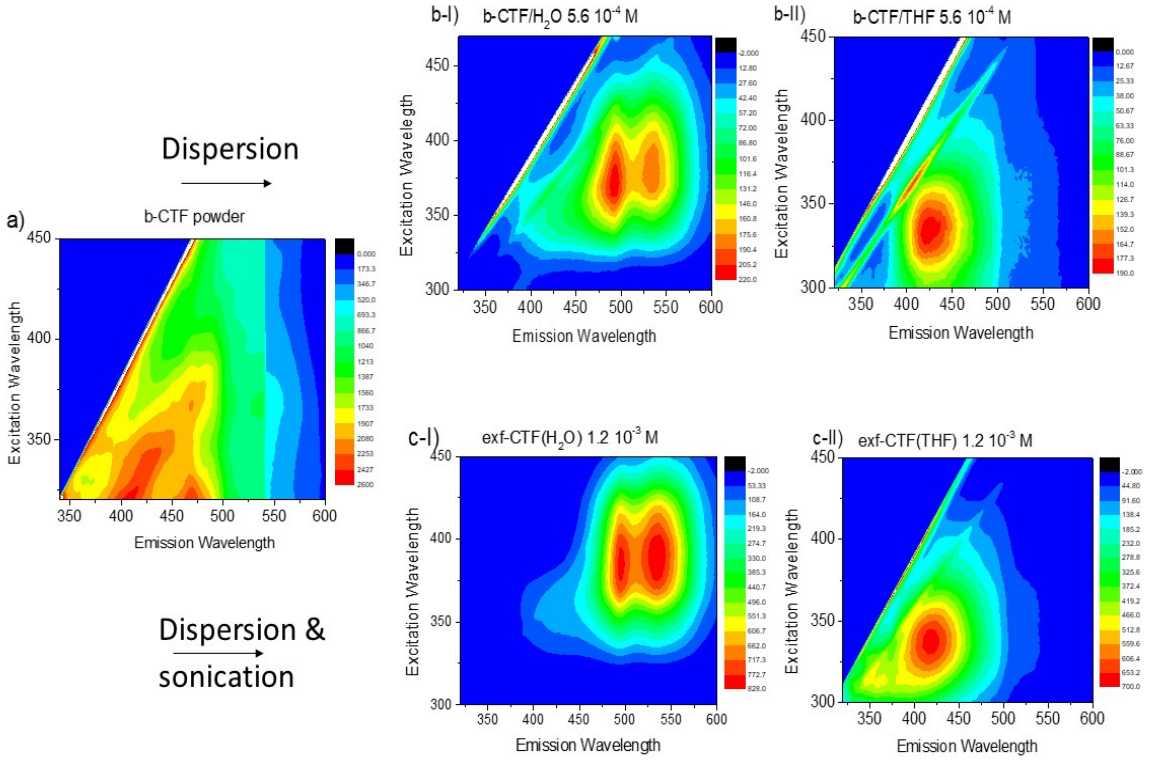

Figure 4. Excitation dependent photoluminescence maps for the a) bulk CTF in the solid state, b I-II) bulk samples dispersed in THF and H_2O, c I-II) dispersions of exfoliated CTF in THF and H_2O.

Light emitting properties in different environments. The effect of concentration and addition of analytes.

The excitation and emission states are recorded by means of fluorescence spectroscopy in solid and liquid state. The spectra were recorded in different solvents, concentrations and redox states and we distinguished the parameters affecting photon emission of the CTF. The typical green emission at λ_{max}=520 nm of a methyl viologen dication MV^{2+} is induced with a photoexcitation centred at λ_{max}=400 nm[59] and in addition, it is proposed that the existence of the shorter wavelength emission band is assigned to a planar reduced viologen, whereas the longer wavelength emission is attributed to the twisted bond connecting its 2 pyridine rings of the radical viologen[60].

In Figure 4, the excitation dependent photoluminescence maps of the b-CTF are presented in the solid state (Figure 4a) and in its different dispersions (Figure 4b for the b-CTF in H_2O and THF and 4c for the exf-CTF in H_2O and THF). The powder of b-CTF (Figure 4a) is consisted of aggregated configurations which can generate a wide range of quenched multi-emissions across ultraviolet and visible range, in contrast to its properties in the liquid state (Figure 4), where the dispersions of the b-CTF in H_2O and THF have a higher efficiency at specific excitation and emission wavelengths.

The π-conjugated polymeric system is highly dependent on the surrounding liquid environment, as a slight change in the polarity of the solvent causes additional shift in the excitation and emission wavelengths. A first comparison is made for the impact on the 5.6×10-4 M b-CTF dispersed in the polar H_2O and the b-CTF dispersed in the aprotic, non-polar THF (Figure 4b-I and 4b-II). The excitation dependent fluorescence map of the b-CTF in a THF dispersion (Figure 4b-II), revealed that b-CTF has an emissive behaviour, identical to the pattern observed on 4,4' bipyridine with an emission maximum at 426 nm (λexc=334 nm). However, in aqueous dispersion, a dual emission response is observed (Figure 4b-I). In this case, the transitions are red shifted at the maximum excitation of 378 nm with two vibronic emissions at λem=494 and 534 nm, accounting a great red Stokes shift. The dual emission exists due to the increased polarity and the capacity of water to offer hydrogen and hydroxyl moieties, by means of protonation storage and oxidative efficiency. The surrounding medium of H_2O lowers the energy of photoexcitation in comparison to the THF medium[55] and the induced intramolecular transfer of the charged counter

ion in THF happens more slowly[61]. The combination of the stabilization of the excited states with radicals and ground states and the creation of excimers with smaller band gap in H_2O facilitate e^- delocalization and the intramolecular charge transfer from bipyridine to triazine units. Additionally, the formation of another charge-transfer complex, consisting of ground state oxidative bipyridine moieties and hydroxide ions when a water molecule transfers a proton to the bulk solvent, could also be the reason for the shift of the excitation maximum from 334 nm (b-CTF/THF) to 378 nm (b-CTF/H_2O)[57]. Following the formation of the charge transfer complex, the charge distributions at the edges of the valence and conduction bands of covalent triazine frameworks exhibit more delocalized electrons on the p_x and p_y orbitals of nitrogen atoms. This leads to a shrinkage of the band gap and can be attributed to the interlayer coupling of valence electrons as demonstrated by Jiang et al[62].

The absolute quantum yield value for the b-CTF dispersed in H_2O at λ_{exc}=370 nm is 3.1×10^{-4}. However, a higher value of 8.2×10^{-3} is calculated for the b-CTF in THF at λ_{exc}=330nm. The results from the fitting are presented in Table S1[63] (Figure S14, Table S1). Unfortunately, the promoted spatial separation of electrons and holes first in H_2O and then THF, results in the decrease of their recombination rate. This is in agreement with the excited-state quenching mechanism for the small Lewis acid molecule of methyl viologen[57]. As far as the exfoliated CTFs in H_2O and THF are concerned, excitation and emission positions follow the same behaviour as b-CTF in each solvent. In the exfoliated materials, quantum efficiencies are enhanced compared to the b-CTF dispersed in H_2O and various non-radiative pathways are blocked[64]. Hence, there are changes in the electronic structure and in the fluorescence mapping from the bulk to the quasi 2D CTFs.

Emissions could be easily tailored by altering the solvent, according to the requirements of the desired application. Furthermore, the aim is to identify whether the optical properties are also influenced by the concentration of the material dispersed in the solvents (Figure 5a-I to 5a-IV & Figure S15 and S19). It has been previously established[65] with 2-/2,6-aryl substituted BODIPY dyes, that at higher concentration the emission shifts to longer wavelengths due to the formation of J-aggregates and later on of the excimers. To validate this behaviour, the fluorescence maps of a gradual dilution of a b-CTF/H_2O are presented in Figure 5a-I to a-IV, where the signal is blue shifted with the decrease of the concentration. A similar study of the fluorescence dependence on the concertation of the exf-CTF(THF) and exf-CTF (H_2O) solutions is presented in Figure S15 and S16. The influence of the induced aggregation in H_2O dispersions on the fluorescence intensity and emission maximum was also tested when SDS was added in excess into the 1.7 M b-CTF dispersion in H_2O. Its excitation and emission maximums were tracked at 330 nm and 430 nm, respectively (Figure S17) and were blue shifted in comparison with the net b-CTF/H_2O with the same concentration (Figure 5a-II), but in accordance with the revised diluted system (Figure 5a-IV). The hydrophobic surfactant tail was imposed in between the layers of the bulk CTF or bonded to its edges. The peak which appeared at 3.1 nm in the XRD pattern (Figure S17) confirmed the increase of the in-plane porosity and the lack of π interactions leading to an unconstrained electron transfer[30]. In the presence of the surfactant, the closer rearrangement of the multimers was inhibited in the H_2O dispersions of high concentrations. Consequently, the optical path of the excited electrons in the liquid phase is highly dependent of the concentration of the dispersed b-CTF.

Experiments after three minutes of constant UV irradiation of the aqueous dispersion of the b-CTF/H_2O with concentration of 5.6×10^{-4} M provoked an induced fluorescence, focusing the emission maximum at 475 nm (λ_{exc}=372 nm), with the second peak fading at 534 nm (purple coloured dispersion, Figure 5b-I). Yet, the irradiation of the b-CTF/THF resulted in the increase of the emission intensity at 426 nm without any shift of the excitation and emission wavelength (clear dispersion, Figure 5b-II). In both the absorbance and fluorescence spectra, the influence of UV irradiation used for the dispersion of b-CTFs in

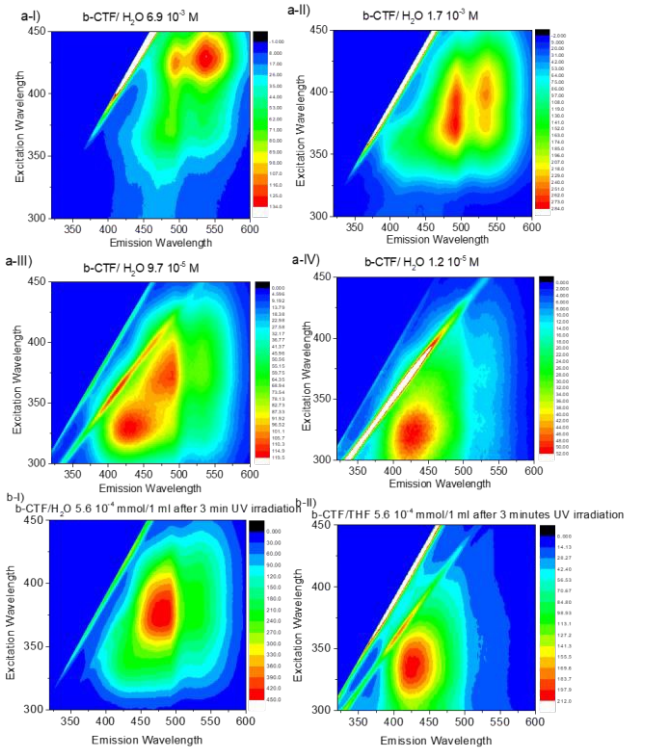

Figure 5 a I-IV) Excitation dependent fluorescence mapping of the bulk-CTF at different concentrations. b-I) Fluorescence mapping of 5.6×10^{-4} M b-CTF in H_2O and b-II) in THF after UV irradiation for 3min

H_2O and THF were studied, thoroughly. The formation of free radicals along with the phenomenon of dimerization, the creation of intermediate gaps and the electron delocalization interfere vastly with the optical properties of the CTF in H_2O.

We further observed that at the lower concentrated (1.2×10^{-5} M) of b-CTF aqueous dispersion, the ultraviolet irradiation led to a red shift of the transitions (λ_{exc}=362nm and λ_{em}=438nm) as can be seen in Figure S19. This confirms the stability of excited states at longer wavelengths along with the formation of free radicals and dimers. The UV irradiation of the dispersions, regardless of the concentration, concentrates the transitions

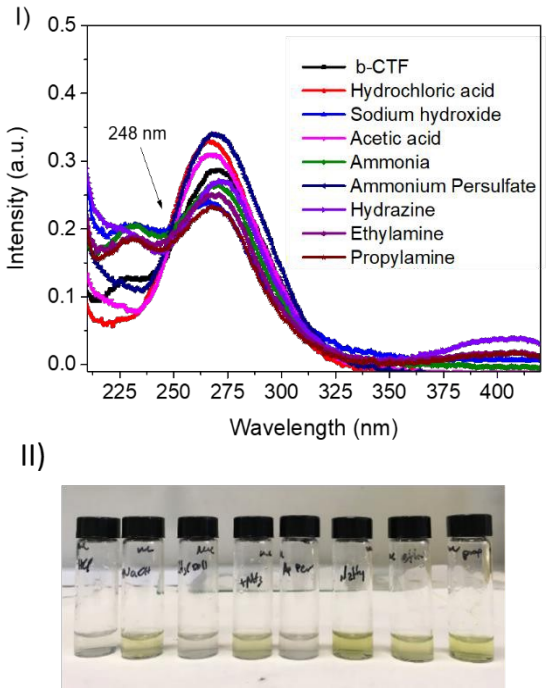

Figure 6. I) Absorbance spectra of b-CTF at a concentration of 2.2×10^{-5} M after the additions of acids or bases at a molecular equivalence. II) Photos of the networks in aqueous dispersions after the additions of the analytes.

near λ_{exc}=370 nm for the excitation and near λ_{em}=440 nm for the emission, also increasing the fluorescence intensity.

CTFs with bipyridine ligands possess a low-energy LUMO, and hence they can undergo charge transfer as electron acceptors in the presence of electron donors such as ammonia and organic amines[7,66]. Additionally, protonation and deprotonation processes have a great influence on the frontier orbitals and the resultant emission[67,68]. The permanent quadrupole moment of s-triazine interacting favourably with both anions (anion-σ backbone of the heteroaromatic ring) and cations (cation-π electrons), are also aspects interfering with the optical response of the CTF[69]. For example, the electrostatic bonding between C_3N_3 and the electronegative part of molecules such as water. Moreover, the s-triazine unit has the ability to develop H-bond networks by its nitrogen, therefore a protonation is plausible[4,70,71,72] and more likely to occur first, as pka of triazine is smaller than the one of bipyridine. The addition of HCl to a high concentrated b-CTF dispersion confirms the above suggestion, since its FTIR spectrum shows two new peaks at 3188 cm^{-1} and 3174 cm^{-1}, attributed to vibrations of -NH and -NH_2 vibrations of the aromatic rings (Figure S19). To that end, we recorded the excitation dependent fluorescence maps with the addition of reagents in two different concentrated aqueous dispersions.

UV-Visible absorbance spectra of 5.6×10^{-4} M b-CTF and 2.2×10^{-5} M b-CTF in H_2O, before and after the addition of reagents in molecular equivalence, are obtained in the range of 200-800 nm wavelength (Figure 6-I). At the low wavelengths (200-400 nm) of the diluted dispersion (Figure 6-I), some differences can be observed that lead to the clarification of whether the nature of the absorbance is driven by the bipyridine or the triazine unit of the b-CTF. Based on the literature, 4,4' bipyridine in liquid state has its maximum peak of absorption at 240 nm (π-π*) and 270 nm (n-π*). On the other hand, the 1,3,5 triazine ring absorbs at 270 nm. Generally, both the bipyridine and triazine units contribute to the b-CTFs/H_2O absorbance spectra, but their quantitative percentage of participation is not clear here. Its initial color of b-CTF/ H_2O is light green. When NaOH, NH_3, N_2H_4 and different amines are added to the dispersions, 4,4' bipyridine absorption signal of the b-CTF is enhanced at 240 nm. The addition of basic molecules induces the π-π* transitions and also a chemical change to its reduced form. This is indicated by the more pronounced peak at λ_{max}=410 nm (Figure 6-I)[73,74] and the final, yellow coloured dispersion[57]. On the contrary, acidic, and oxidative additions influence the absorption signal of the triazine unit of the b-CTF at 270 nm, indicating a chemical change at its environment. When the b-CTF is found in acidic and oxidizing environments, the dispersion in H_2O is transparent. In consequence, the visible change on the colour of the dispersions reflects to the redox state of the b-CTF/H_2O.

The addition of the bases and reducing reagents in b-CTF/H_2O favours the increase of the blue shifted emissive species as seen in fluorescence maps, whereas acids and oxidative agents lead to the fluorescence quenching and the red shift of excitation and emission wavelengths. The same performance was tracked in THF dispersions, where a great improvement of the fluorescence signal was observed with the introduction of the aliphatic amines, donating its lone pairs and reducing at the same time the CTFs[75] (Figure S21). The fluorescence mapping for the two different concentrations of b-CTF dispersions after the addition of reagents in both molecular equivalence and excess are presented in Figures S20-S24. The summary of the results can be seen at the fluorescence response chart into the diluted dispersion in Figures 7 I and the fluorescence response chart of the highly concentrated b-CTF dispersion in H_2O is given in Figure S25.

The guest molecules found in excess in the 2.2×10^{-5} M b-CTF aqueous dispersions brought similar results with the ones found for the molecular equivalence additions as long as the positions (range for excitation from 300 to 320 nm and for the emission from 360 nm to 430 nm, depending on the case) and the intensity of emission are concerned (Figure S24, Figure S25). For the denser b-CTF aqueous dispersion of 5.9×10^{-4} M, the excitation can be tuned from 320 nm to 400 nm and the emission from 425 nm to 550 nm according to the addition (Figure S25). Based on the presented charts, fluorescence intensity becomes stronger in neutral (with the reducing agent of hydrazine) and basic environments than in acidic. One of the reasons would be that nitrogen atoms were protonated at lower pH, thus leading to the deactivation of one of the emissive states[76], with the reduced b-CTF requiring a higher energy for excitation without any quenching mechanisms at the emission path.

From these results, a pattern can be developed for the recognition of small ions in coherence with the redox states of the CTFs. Excited states of the dications are red shifted (excitation at 3.35 eV and emission at 2.4 eV) in comparison with the radical species (excitation at 3.35 eV and emission at 2.5 eV) and the reduced ones (excitation at 3.6 eV and emission at 2.8 eV). In basic/reducing environments 4,4 bipyridine seems to have a more crucial role on the emission, whereas in acidic/oxidising environments, triazine units influence the fluorescence response more. Hydrolysis of the CTF shifted the excitation and emission at longer wavelengths, a response that could be modulated with the addition of specific reagents. UV illumination of the dispersions promoted a high fluorescence emission in both H_2O and THF. The formation of aggregates and excimers is highly dependent on the concentration of the dispersions. And lastly, the recombination rate of charges in the CTF/H_2O dispersions was enhanced in reducing environments and basic solutions, whereas spatial charge separation was induced in oxidative environments and acidic solutions, as fluorescence intensity is quenched.

Time resolved fluorescence measurements.

Time resolved photoluminescence measurements from 5 to 300 K were performed to elucidate the emission kinetics of the b-CTF, exf-CTF(H_2O) and exf-CTF(THF) on Si wafers. Photoluminescence lifetime profiles for 5K and 300K are displayed in Figure 8 a-c and a summary plot of the lifetimes is presented in Figure 8d. The decay curves of all measurements fitted well with mono-exponential decay function. The lifetime of the bulk network is shorter in comparison with the exf-CTF(H_2O) and it is longer in comparison with exf-CTF(THF) at both low and room temperature. The plot summary of the lifetimes at temperatures from 5 to 300 K reveals also that shorter decays appear when we tend to approach the ambient conditions. At lower temperatures, it is well documented that fluorescence emission and lifetime increase for semiconducting materials[77].

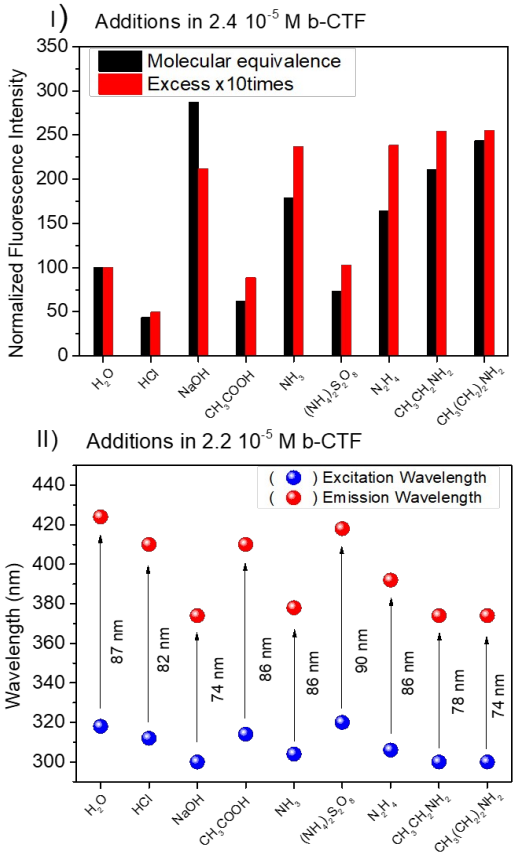

Figure 7. I) Emission response chart for various analytes. II) Excitation and emission positions maxima.

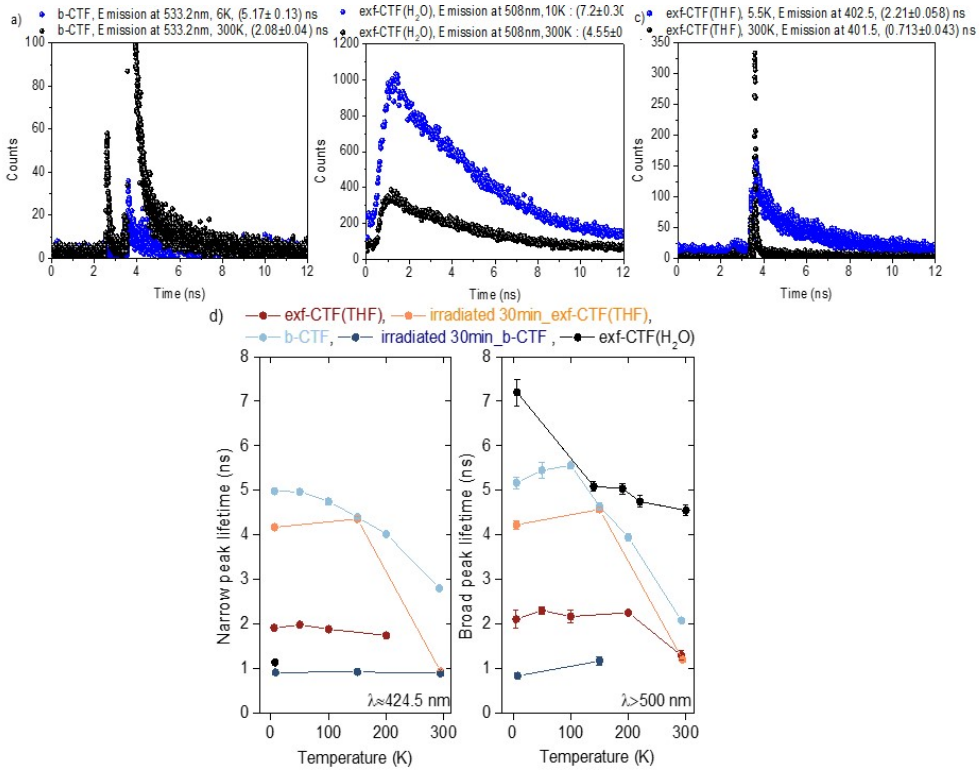

Figure 8. Lifetime profiles of a) b-CTF, b) exf-CTF(H_2O), c) exf-CTF(THF) at a low temperature and RT, d) Lifetimes of all samples depending on the temperature and the peak of the emission.

All the samples excited at wavelengths from 370 to 405 nm had three main emission peaks in the range of 410-550 nm, with the most prevailing lifetime at the green wavelengths (Figure 8d), albeit with lower intensity. One possible explanation would be the excimer formation[65,78], while at the same time, the existence of trap states on the visible region is also reported[79]. The latter is in accordance with our UV-visible spectroscopy results and the suggestion about the formation of internal states upon illumination of our samples treated in H_2O. Questions arise regarding the lifetime of the CTF exfoliated in THF which is characterized by a shorter decay than the exfoliated CTF in H_2O. One reason is that the sample hadn't been excited at its maximum wavelength at λ_{exc}=330 nm due to instrument limitations. Moreover, a long pass filter from 390 to UV was used for the measurements and it can be correlated with the low intensity emission in Figure 8c. Despite the practical issues, one interpretation of the results would be that it's opaque morphology may not favour stabilization of the excited states, as recombination and charge efficiency were higher than those of the exf-CTF(H_2O), depending on the calculated quantum yield.

The UV treated b-CTF loses its long-lived lifetimes throughout the whole temperature and emission range, whereas for the UV

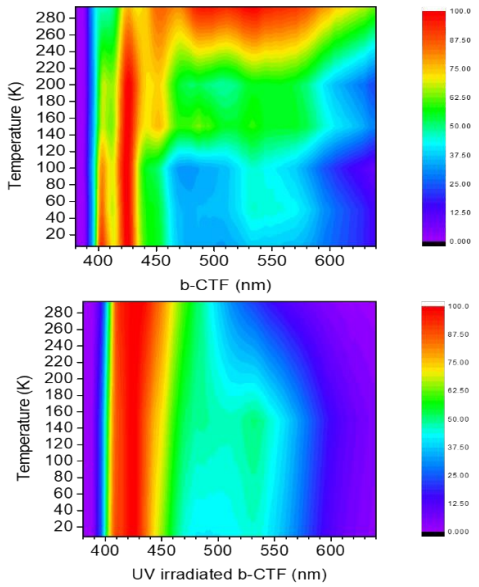

Figure 9. Heat maps of the b-CTF emission depending on the temperature, before and after irradiation of 30min.

irradiated exf-CTF(THF), there is a positive effect on the lifetime which is doubled at low temperatures. For the UV irradiated b-CTF, more studies have to be conducted in order to identify if there is a faster recombination rate or if the induced radicals of the b-CTF can reduce the present oxygen species.
Lastly, in Figure 9, PL intensity of b-CTF is presented depending on the temperature and the emission wavelength. Between non-treated and treated with irradiation b-CTF at RT, we can observe a blue shift of the emissions and the decrease of the ones found at 450-600nm, as discussed also in the previous section. Instead, low temperatures, mask many non-radiative pathways and for the UV irradiated b-CTF, emissions at 450-550nm start to enhance from 200K to 5K. The UV irradiation induces the intensity of the exf-CTF(THF) at all temperatures (Figure S26).

Conclusions

In this work, we report the effect of chemical and mechanical liquid exfoliation of covalent triazine frameworks on their light emitting properties by means of steady state and time resolved fluorescence measurements. Firstly, we proved that substantial changes in the conformation and morphological characteristics of the networks are caused by the exfoliation process and have pronounced effects on their optical properties. A substantial increase on the emission and their lifetimes after exfoliation was observed. Furthermore, the dispersion of the networks to polar and non-polar solvents was found to influence their vibronic and emissive states. A correlation of the redox states with their fluorescence patterns was defined through careful additions of a series of analytes. Lastly, UV irradiation affects the optical properties of the CTF regarding not only their adsorption and emission, but also their lifetimes at different temperatures.

Conflicts of interest

There are no conflicts to declare.

Acknowledgements

P.B & P.D would like to acknowledge the General Secretary for Research and Innovation and the Hellenic Foundation for Research and Innovation grant number 1468 “Plascat”.

Notes and references

1 C. R. Zhu, J. F. Long, Q. Tang, C. Bin Gong and X. K. Fu, *J. Appl. Electrochem.*, 2018, **48**, 1121–1129.
2 X. D. Yang, R. Zhu, J. P. Yin, L. Sun, R. Y. Guo and J. Zhang, *Cryst. Growth Des.*, 2018, **18**, 3236–3243.
3 P. M. S. Monk, D. R. Rosseinsky and R. J. Mortimer, *Electrochromic Mater. Devices*, 2015, 57–90.
4 R. Kulkarni, Y. Noda, D. Kumar Barange, Y. S. Kochergin, P. Lyu, B. Balcarova, P. Nachtigall and M. J. Bojdys, *Nat. Commun.*, 2019, **10**, 3228.
5 M. Huang, J. Chong, C. Hu and Y. Yang, *Inorg. Chem. Commun.*, 2020, **119**, 108094.
6 H. S. Jung, P. Verwilst, W. Y. Kim and J. S. Kim, *Chem. Soc. Rev.*, 2016, **45**, 1242–1256.
7 W. Shi, F. Xing, Y. L. Bai, M. Hu, Y. Zhao, M. X. Li and S. Zhu, *ACS Appl. Mater. Interfaces*, 2015, **7**, 14493–14500.
8 Y. Liu, Y. Ma, J. Yang, C. S. Diercks, N. Tamura, F. Jin and O. M. Yaghi, *J. Am. Chem. Soc.*, 2018, **140**, 16015–16019.
9 L. Li, Y. Zhu, N. Gong, W. Zhang, W. Peng, Y. Li, F. Zhang and X. Fan, *Int. J. Hydrogen Energy*, 2020, **45**, 2689–2698.
10 H. J. Zhu, M. Lu, Y. R. Wang, S. J. Yao, M. Zhang, Y. H. Kan, J. Liu, Y. Chen, S. L. Li and Y. Q. Lan, *Nat. Commun.*, 2020, **11**, 497.
11 J. Chen, X. Tao, C. Li, Y. Ma, L. Tao, D. Zheng, J. Zhu, H. Li, R. Li and Q. Yang, *Appl. Catal. B Environ.*, 2020, **262**, 118271.
12 L. Z. Peng, P. Liu, Q. Q. Cheng, W. J. Hu, Y. A. Liu, J. S. Li, B. Jiang, X. S. Jia, H. Yang and K. Wen, *Chem. Commun.*, 2018, **54**, 4433–4436.
13 Z. Lei, Q. Yang, Y. Xu, S. Guo, W. Sun, H. Liu, L. P. Lv, Y. Zhang and Y. Wang, *Nat. Commun.*, 2018, **9**, 576.
14 X. Liu, C. F. Liu, W. Y. Lai and W. Huang, *Adv. Mater. Technol.*, 2020, **5**, 2000154.
15 X. He, Y. Yang, H. Wu, G. He, Z. Xu, Y. Kong, L. Cao, B. Shi, Z. Zhang, C. Tongsh, K. Jiao, K. Zhu and Z. Jiang, *Adv. Mater.*, 2020, **32**, 2001284.
16 Y. Gao, C. Zhi, P. Cui, K. A. I. Zhang, L. P. Lv and Y. Wang, *Chem. Eng. J.*, 2020 ,125967.
17 M. A. Gatou, P. Bika, T. Stergiopoulos, P. Dallas and E. A. Pavlatou, *Energies*, 2021, **14**, 3197.
18 K. Wang, L. M. Yang, X. Wang, L. Guo, G. Cheng, C. Zhang, S. Jin, B. Tan and A. Cooper, *Angew. Chemie - Int. Ed.*, 2017, **56**, 14149–14153.
19 Y. Y. Liu, X. C. Li, S. Wang, T. Cheng, H. Yang, C. Liu, Y. Gong, W. Y. Lai and W. Huang, *Nat. Commun.*, 2020, **11**, 5561.
20 P. Li, L. J. Zhou, N. N. Yang, Q. Sui, T. Gong and E. Q. Gao, *Cryst. Growth Des.*, 2018, **18**, 7191–7198.
21 S. L. Li, M. Han, B. Wu, J. Wang and X. M. Zhang, *Cryst. Growth Des.*, 2018, **18**, 3883–3889.
22 Q. Sui, X. T. Ren, Y. X. Dai, K. Wang, W. T. Li, T. Gong, J. J. Fang, B. Zou, E. Q. Gao and L. Wang, *Chem. Sci.*, 2017, **8**, 2758–2768.
23 S. Hug, M. E. Tauchert, S. Li, U. E. Pachmayr and B. V. Lotsch, *J. Mater. Chem.*, 2012, **22**, 13956–13964.
24 L. Striepe and T. Baumgartner, *Chem. - A Eur. J.*, 2017, **23**, 16924–16940.
25 A. di Matteo, *Chem. Phys. Lett.*, 2007, **439**, 190–198.
26 J. S. Costa, A. G. Castro, R. Pievo, O. Roubeau, B. Modec, B. Kozlevčar, S. J. Teat, P. Gamez and J. Reedijk, *CrystEngComm*, 2010, **12**, 3057–3064.
27 Y. Yu, G. Li, J. Liu and D. Yuan, *Chem. Eng. J.*, 2020, **401**, 126139.
28 W. R. Cui, C. R. Zhang, W. Jiang, R. P. Liang and J. D. Qiu, *ACS Appl. Nano Mater.*, 2019, **2**, 5342–5349.
29 G. S. Kumar and D. C. Neckers, *Chem. Rev.*, 1989, **89**, 1915–1925.
30 A. B. Bourlinos, P. Dallas, Y. Sanakis, D. Stamopoulos, C. Trapalis and D. Niarchos, *Eur. Polym. J.*, 2006, **42**, 2940–

2948.
31 T. Giannakopoulou, I. Papailias, N. Todorova, N. Boukos, Y. Liu, J. Yu and C. Trapalis, *Chem. Eng. J.*, 2017, **310**, 571–580.
32 P. M. S. Monk and N. M. Hodgkinson, *Electrochim. Acta*, 1998, **43**, 245–255.
33 T. Kobayashi and T. Ichikawa, *Materials*, 2017, **10**, 1243.
34 J. Romanova, V. Liégeois and B. Champagne, *Phys. Chem. Chem. Phys.*, 2014, **16**, 21721–21731.
35 J. Romanova, V. Liégeois and B. Champagne, *J. Phys. Chem. C*, 2014, **118**, 12469–12484.
36 M. L. Główka, D. Martynowski and K. Kozłowska, *J. Mol. Struct.*, 1999, **474**, 81–89.
37 C. Janiak, *J. Chem. Soc. Dalt. Trans.*, 2000, 3885–3896.
38 Y. Wang, H. D. Tran, L. Liao, X. Duan and R. B. Kaner, *J. Am. Chem. Soc.*, 2010, **132**, 10365–10373.
39 A. N. Parikh, M. A. Schivley, E. Koo, K. Seshadri, D. Aurentz, K. Mueller and D. L. Allara, *J. Am. Chem. Soc.*, 1997, **119**, 3135–3143.
40 Y. B. Zhang, J. Su, H. Furukawa, Y. Yun, F. Gándara, A. Duong, X. Zou and O. M. Yaghi, *J. Am. Chem. Soc.*, 2013, **135**, 16336–16339.
41 N. Zhang, T. Wang, X. Wu, C. Jiang, F. Chen, W. Bai and R. Bai, *RSC Adv.*, 2018, **8**, 3803–3808.
42 G. Das, T. Skorjanc, S. K. Sharma, F. Gándara, M. Lusi, D. S. Shankar Rao, S. Vimala, S. Krishna Prasad, J. Raya, D. S. Han, R. Jagannathan, J. C. Olsen and A. Trabolsi, *J. Am. Chem. Soc.*, 2017, **139**, 9558–9565.
43 L. Zhang, T. Y. Zhou, J. Tian, H. Wang, D. W. Zhang, X. Zhao, Y. Liu and Z. T. Li, *Polym. Chem.*, 2014, **5**, 4715–4721.
44 C. Chen, J. K. Sun, Y. J. Zhang, X. D. Yang and J. Zhang, *Angew. Chemie - Int. Ed.*, 2017, **56**, 14458–14462.
45 P. Peng, L. Shi, F. Huo, S. Zhang, C. Mi, Y. Cheng and Z. Xiang, *ACS Nano*, 2019, **13**, 878–884.
46 R. J. Jasinski, *J. Electrochem. Soc.*, 1977, **124**, 637.
47 C. L. Bird and A. T. Kuhn, *Chem. Soc. Rev.*, 1981, **10**, 49–82.
48 P.M.S.Monk, R.D.Fairweather, M. D. Ingram and J. A. Duffy. *J. Chem. Soc. Perkin Trans. 2*, 1992, 2039–2041.
49 R. Papadakis, *Molecules*, 2020 , **25**, 1.
50 J. F. Stargardt and F. M. Hawkridge, *Anal. Chim. Acta*, 1983, **146**, 1–8.
51 T. W. and K. Honda, *J. Phys. Chem*, 1982, **370**, 2617–2619.
52 D. Leest, *Electroanal. Chem. Interracial Electrochem.*, 1973, **43**, 251–255.
53 E. E. Engelman and D. H. Evans, *Anal. Chem.*, 1994, **66**, 1530–1534.
54 J. K. Sun, Y. J. Zhang, G. P. Yu, J. Zhang, M. Antonietti and J. Yuan, *J. Mater. Chem. C*, 2018, **6**, 9065–9070.
55 L. Ascherl, E. W. Evans, M. Hennemann, D. Di Nuzzo, A. G. Hufnagel, M. Beetz, R. H. Friend, T. Clark, T. Bein and F. Auras, *Nat. Commun.*, 2018, **9**, 3802.
56 E. M. Kosower and J. L. Cotter, *J. Am. Chem. Soc.*, 1964, **86**, 5524–5527.
57 J. D. Henrich, S. Suchyta and B. Kohler, *J. Phys. Chem. B*, 2015, **119**, 2737–2748.
58 J. Peon, X. Tan, J. D. Hoerner, C. Xia, Y. F. Luk and B. Kohler, *J. Phys. Chem. A*, 2001, **105**, 5768–5777.
59 A. W. H. Mau, J. M. Overbeek, J. W. Loder and W. H. F. Sasse, *J. Chem. Soc. Faraday Trans. 2 Mol. Chem. Phys.*, 1986, **82**, 869–876.
60 A. C. Fahrenbach, Z. Zhu, D. Cao, W. G. Liu, H. Li, S. K. Dey, S. Basu, A. Trabolsi, Y. Y. Botros, W. A. Goddard and J. F. Stoddart, *J. Am. Chem. Soc.*, 2012, **134**, 16275–16288.
61 T.-C. Lin, Z.-Y. Liu, S.-H. Liu, I. O. Koshevoy and P.-T. Chou, *JACS Au*, 2021, **1**, 282–293.
62 X. Jiang, P. Wang and J. Zhao, *J. Mater. Chem. A*, 2015, **3**, 7750–7758.
63 L. T. Jian Yang, Yi Zhang, Santosh Gautam, Li Liu, Jagannath Dey, Wei Chen, Ralph P. Mason, Carlos A. Serrano, Kevin A. Schug and Liping Tang, *Proc. Natl. Acad. Sci. U. S. A.*, 2009, **106**, 11818.
64 A. Splendiani, L. Sun, Y. Zhang, T. Li, J. Kim, C. Y. Chim, G. Galli and F. Wang, *Nano Lett.*, 2010, **10**, 1271–1275.
65 D. Tian, F. Qi, H. Ma, X. Wang, Y. Pan, R. Chen, Z. Shen, Z. Liu, L. Huang and W. Huang, *Nat. Commun.*, 2018, **9**, 2688.
66 T. Škorjanc, D. Shetty, M. A. Olson and A. Trabolsi, *ACS Appl. Mater. Interfaces*, 2019, **11**, 6705–6716.
67 J. Jia and L. Wu, *Org. Electron.*, 2020, **76**, 105466.
68 K. L. VanDenburgh, Y. Liu, T. Sadhukhan, C. R. Benson, N. M. Cox, S. Erbas-Cakmak, B. Qiao, X. Gao, M. Pink, K. Raghavachari and A. H. Flood, *Org. Biomol. Chem.*, 2020, **18**, 431–440.
69 T. J. Mooibroek and P. Gamez, *Inorganica Chim. Acta*, 2007, **360**, 381–404.
70 F. Elbe, J. Keck, A. P. Fluegge, H. E. A. Kramer, P. Fischer, P. Hayoz, D. Leppard, G. Rytz, W. Kaim and M. Ketterle, *J. Phys. Chem. A*, 2000, **104**, 8296–8306.
71 N. Xu, R. L. Wang, D. P. Li, Z. Y. Zhou, T. Zhang, Y. Z. Xie and Z. M. Su, *New J. Chem.*, 2018, **42**, 13367–13374.
72 J. A. Zerkowski, C. T. Seto and G. M. Whitesides, *J. Am. Chem. Soc.*, 1992, **114**, 5473–5475.
73 A. H. Corwin, R. R. Arellano and A. B. Chivvis, *BBA - Bioenerg.*, 1968, **162**, 533–538.
74 C. Chen, H. Rao, S. Lin and J. Zhang, *Dalt. Trans.*, 2018, **47**, 8204–8208.
75 A. Meffre, S. Lachaize, C. Gatel, M. Respaud and B. Chaudret, *J. Mater. Chem.*, 2011, **21**, 13464–13469.
76 Y. Zhu, M. Qiao, W. Peng, Y. Li, Y. Li, G. Zhang, F. Zhang and X. Fan, *J. Mater. Chem. A*, 2017, **5**, 9272–9278.
77 C. Robert, D. Lagarde, F. Cadiz, G. Wang, B. Lassagne, T. Amand, A. Balocchi, A. Renucci, S. Tongay, B. Urbaszek and X. Marie, *Phys. Rev. B,* 2016, **93**, 205423.
78 N. C. Flanders, M. S. Kirschner, P. Kim, T. J. Fauvell, A. M. Evans, W. Helweh, A. P. Spencer, R. D. Schaller, W. R. Dichtel and L. X. Chen, *J. Am. Chem. Soc.*, 2020, **142**, 14957–14965.
79 S. Yang, D. Streater, C. Fiankor, J. Zhang and J. Huang, *J. Am. Chem. Soc.*, 2021, **143**, 1061–1068.